# Observation of Unconventional Dynamics of Domain Walls in Uniaxial Ferroelectric Lead Germanate

*Ohheum Bak, Theodor S. Holstad, Yueze Tan, Haidong Lu, Donald M. Evans, Kasper A. Hunnestad, Bo Wang, James P. V. McConville, Petra Becker, Ladislav Bohatý, Igor Lukyanchuk, Valerii M. Vinokur, Antonius T. J. van Helvoort, J. Marty Gregg, Long-Qing Chen, Dennis Meier,* and Alexei Gruverman**

**Application of scanning probe microscopy techniques such as piezoresponse force microscopy (PFM) opens the possibility to re-visit the ferroelectrics previously studied by the macroscopic electrical testing methods and establish a link between their local nanoscale characteristics and integral response. The nanoscale PFM studies and phase field modeling of the static and dynamic behavior of the domain structure in the well-known ferroelectric material lead germanate, $Pb_5Ge_3O_{11}$, are reported. Several unusual phenomena are revealed: 1) domain formation during the paraelectric-to-ferroelectric phase transition, which exhibits an atypical cooling rate dependence; 2) unexpected electrically induced formation of the oblate domains due to the preferential domain walls motion in the directions perpendicular to the polar axis, contrary to the typical domain growth behavior observed so far; 3) absence of the bound charges at the 180° head-to-head (H–H) and tail-totail (T–T) domain walls, which typically exhibit a significant charge density in other ferroelectrics due to the polarization discontinuity. This strikingly different behavior is rationalized by the phase field modeling of the dynamics of uncharged H–H and T–T domain walls. The results provide a new insight into the emergent physics of the ferroelectric domain boundaries, revealing unusual properties not exhibited by conventional Ising-type walls.**

## 1. Introduction

Piezoresponse force microscopy (PFM) has evolved into a powerful tool for characterizing and manipulating the functional behavior of a wide range of ferroelectrics and related polar materials at the nanometer scale.[1] Along with other scanning probe microscopy (SPM) techniques it enabled the discovery of a series of phenomena, which inspired new fundamental physics and exciting device applications. One of the most notable examples is the observation of electrically conducting domain walls in otherwise insulating ferroic materials, such as magnetoelectric $BiFeO_3$ thin films,[2] improper ferroelectric $ErMnO_3$ crystals,[3] and proper ferroelectric $LiNbO_3$ crystals and films.[4,5] Although many of these materials had been investigated thoroughly for decades, only the application of modern SPM techniques allowed direct assessment of the domain wall properties and better

O. Bak, Dr. H. Lu, Prof. A. Gruverman
Department of Physics and Astronomy
University of Nebraska
Lincoln, NE 68588, USA
E-mail: agruverman2@unl.edu

T. S. Holstad, Dr. D. M. Evans, K. A. Hunnestad, Prof. D. Meier
Department of Materials Science and Engineering
Norwegian University of Science and Technology (NTNU)
Trondheim 7491, Norway
E-mail: dennis.meier@ntnu.no

Y. Tan, Dr. B. Wang, Prof. L.-Q. Chen
Department of Materials Science and Engineering
Pennsylvania State University
University Park PA 16802, USA

J. P. V. McConville, Prof. J. M. Gregg
Centre for Nanostructured Media
School of Mathematics and Physics
Queen's University
Belfast BT7 1NN, UK

Prof. P. Becker, Prof. L. Bohatý
Institute of Geology and Mineralogy
Section Crystallography
University of Cologne
Zulpicher Str. 49b, Cologne 50674, Germany

Prof. I. Lukyanchuk
Laboratory of Condensed Matter Physics
University of Picardie
Amiens 80039, France

Dr. V. M. Vinokur
Materials Science Division
Argonne National Laboratory
9700 S Cass Ave, Lemont, IL 60439, USA

Prof. A. T. J. van Helvoort
Department of Physics
Norwegian University of Science and Technology (NTNU)
Trondheim 7491, Norway

understanding of their complex nanoscale physics providing a strong push forward for the nascent research field of domain-wall nanoelectronics. In general, transition to nanoscale ferroelectric structures provides a tangible reason for re-visiting the ferroelectrics previously studied by the macroscopic electrical testing methods to establish a link between their local properties and integral response and tackle the behavior of ferroelectric domains and domain walls with unprecedented completeness.

Here, we report nanoscale PFM studies of the static and dynamic behavior of the domain structure, driven both by temperature and electric fields, in the well-known ferroelectric material lead germanate, $Pb_5Ge_3O_{11}$ (PGO).[6,7] Lead germanate is a model system for the study of the fundamental mechanisms related to the nucleation and sideways growth of ferroelectric domains.[8,9] Up to now, these processes have been investigated by optical methods that allow monitoring of the domain structure evolution on the polar surface. However, the domain growth along the polar direction has not been addressed so that the full 3D switching behavior of this ferroelectric system remains unclear. In this study, we combine PFM measurements and phase field modeling to investigate the static and dynamic properties of the ferroelectric domain structure in lead germanate at the nanoscale. We obtain a new insight into the domain formation during the paraelectric-to-ferroelectric phase transition as well as into the switching dynamics on the non-polar surface. Our study reveals an unusual asymmetry in the motion of domain walls in the directions parallel and perpendicular to the polar axis, which we attribute to another very unusual characteristic of PGO: the absence of bound charges at the 180° head-to-head (H–H) and tail-to-tail (T–T) domain walls.

Ferroelectricity in PGO was first reported at the beginning of the 1970s, featuring a threefold polar axis along the [001] crystallographic axis.[7,10] This material exhibits a remnant polarization of $P = 4.8\ \mu C\ cm^{-2}$, which arises across a second order phase transition at 177 °C where the space group symmetry changes from $P\bar{6}$ (paraelectric phase) to $P3$ (ferroelectric phase). One of the most peculiar characteristics of PGO is its polarization-dependent optical activity; as a consequence, the optical rotatory power switches from a left-handed system to a right-handed one and vice versa when the polarization direction is reversed.[11] This feature of PGO allows straightforward observation of the domain structure in polarized light,[12] which has been extensively used to resolve the field-induced domain dynamics during polarization reversal.[8,13]

In this study, we use single crystals of PGO grown either by the Czochralski method or by the top-seeded Nacken-Kyropoulos method using the [001] direction as seed crystal orientation in both cases. The samples have been oriented and cut with a diamond saw normal to the polar axis (with the polar surface corresponding to the (001) plane). The resulting parallel-plane plates are several square millimeters in size and have a thickness of about 0.5 mm. Mechanical polishing is applied to achieve surfaces with optical quality. Cutting along the (100) and (010) planes has been used to obtain samples with non-polar surfaces (x-cut). Control experiments have been performed using the samples with freshly cleaved surfaces. PFM imaging has been performed by using commercial atomic force microscopy (AFM) systems (MFP-3D and Cypher ES, Asylum Research) with conductive Pt/Ir coated tips (PPP-EFM, Nanosensors). An ac modulation voltage of 9 V at frequency of 8–15 kHz was applied to the tip, with an external lock-in amplifier used for signal processing. Switching voltage was supplied to the tip via a Keithley source/measurement unit (Model 237).

## 2. Results and Discussion

The as-grown domain structure in PGO, revealed by PFM and shown in **Figure 1**, reflects the uniaxial ferroelectricity of the material. The vertical PFM scan obtained on the polar surface (Figure 1a) displays a pattern of irregular domains with antiparallel out-of-plane polarization directions. In contrast, a lateral PFM image acquired on the non-polar surface shows a pattern of domains elongated along the [001] polar axis (Figure 1b). Similar domain arrangements have been observed in all samples irrespective of the surface preparation methods (Figure S1, Supporting Information). An isometric illustration of the as-grown domain arrangement in Figure 1c displays a difference in characteristic domain size along different crystallographic directions. This arrangement is consistent with the propensity of proper ferroelectrics to form neutral 180° domain walls to avoid the emergence of bound charges. However, in addition to the neutral 180° domain walls (type I in Figure 1b), there are also sections of the domain boundaries that correspond to the H–H and T–T arrangements (types II and III in Figure 1b, respectively). This observation, which corroborates the previously reported domain data obtained by selective etching,[13] presents PGO as a unique example of a uniaxial proper ferroelectric that readily develops nominally charged domain walls at the micrometer length scale in the as-grown state.

To gain an insight into the formation of this unusual domain structure, we performed a cooling-rate-dependent investigation of the domain structure. The experiments were carried out in situ using a Cypher ES AFM, which allowed both atmospheric and temperature control. The sample chamber was flushed multiple times with $N_2$ before heating the sample to 250 °C in a constant flow of nitrogen. It was then cooled through the phase transition to room temperature at different rates in the range between 0.01 and 2 °C $s^{-1}$. PFM images of the non-polar surface were acquired at room temperature after the sample temperature had equilibrated. No change in the sample surface topography was observed upon repeated thermal cycling.

The PFM images acquired on the non-polar (010) surface reveal a strong dependence of the in-plane domain arrangement on the cooling rate (**Figure 2**). Auto-correlation analysis of the PFM data (see Section S2, Supporting Information, for details) provides a quantitative insight into the observed evolution of the domain size (Figure 2a). The correlation length, which gives a measure of the characteristic domain size, is found to be monotonically increasing as the cooling rate is increased (Figure 2b). In addition, the higher cooling rates result in stronger anisotropy of the correlation length consistent with the fact that the domains become larger along the polar [001] direction resembling the as-grown domain structure (Figure 1).

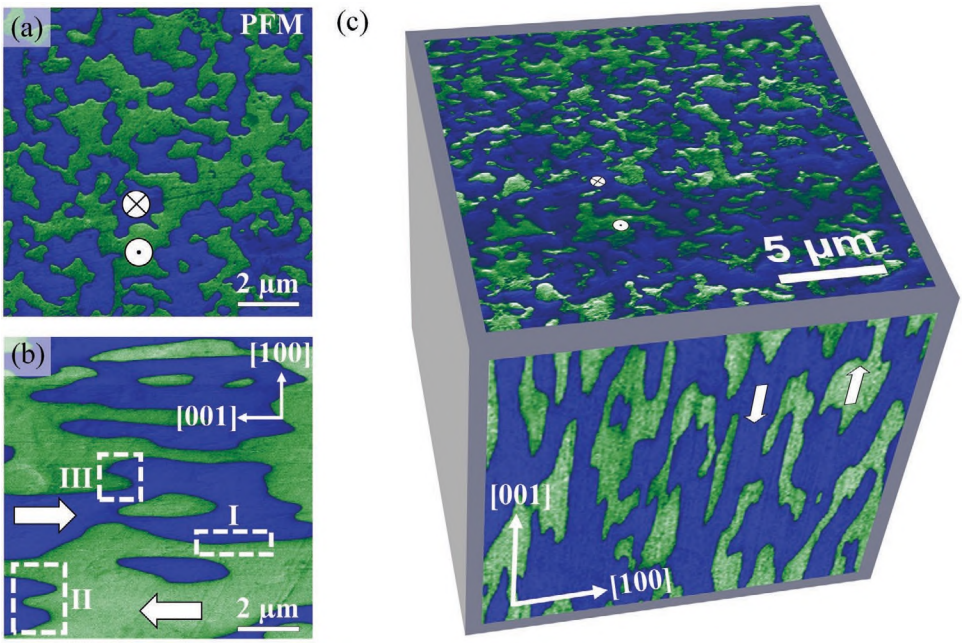


**Figure 1.** PFM imaging of the ferroelectric domain structure in the as-grown $Pb_5Ge_3O_{11}$ crystal. a) Vertical PFM phase image of the out-of-plane polarization acquired on the polar surface. b) Lateral PFM phase image of the in-plane polarization obtained on the non-polar surface. White arrows indicate polarization directions and dashed frames indicate different types of domain walls: neutral 180° (I), H–H (II), and T–T (III). c) Illustration of 3D domain geometry. In the as-grown state, $Pb_5Ge_3O_{11}$ displays a strongly anisotropic domain arrangement manifested by domain elongation along the polar [001] axis. PFM images of the polar surface in (a) and (c) were collected from the sample cut from the same single crystal used for non-polar surface imaging shown in (b) and (c) as well as in Figure 2. All the data in Figure 1 were collected prior to any thermal treatment.

It should be noted that the observed evolution of the correlation length with the varying cooling rate is opposite to the earlier reports on the effect of quenching on the domain size. Both the experimental data[14–16] and the predictions within the framework of the Lifshitz–Allen–Cahn theory[17,18] indicate that the evolution of the domain size $R$ as a function of the cooling rate is best described by the power-law $R \approx r^{-\mu}$, where $r$ is the cooling rate and $\mu$ is a universal exponent. From the general point of view, formation of domains during a phase transition is driven by the need of the system to minimize its depolarizing energy by eliminating the net polarization charges at the sample surface or at the structural defects. At the transition point, domains nucleate due to the fluctuations between the para- and ferroelectric phases. For very fast cooling rates, the nucleated domains will get frozen well below the transition point and the domain size will be small. On the other hand, it has been reported that the inverse scaling as a function of the cooling rate occurred at the transition between two fluctuation regimes (Ginzburg and mean field) in hexagonal manganites.[19] Whether this transition regime or charged defects, a pyroelectric field,[20] or unusual domain wall properties are responsible for the unexpected inverse cooling rate dependence

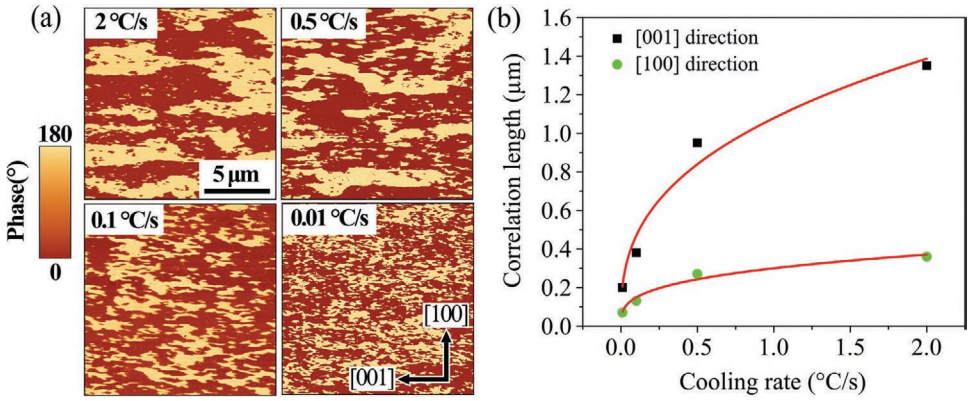


**Figure 2.** a) Lateral PFM phase images (sensing the [001] direction) of the domain patterns acquired at room temperature on the non-polar surface of $Pb_5Ge_3O_{11}$ after cooling from 250 °C through the phase transition with different cooling rates. Each of the scans comes from an adjoining area, taken on the same single crystal used in Figure 1. b) Correlation lengths in the [001] and [100] directions as a function of the cooling rate. The red lines are guides to the eye.

of the domain size remains to be clarified. What is important is that the observed atypical cooling-rate-dependent behavior is part of the overall non-trivial domain wall dynamics in PGO.

After observing the unusual temperature-driven domain formation, we investigated the electric field driven dynamics of the ferroelectric domains to an electric field focusing on the non-polar surface of PGO that had not been subjected to thermal treatment. These studies have been carried out by measuring the size of the switched domains as a function of the amplitude and duration of the voltage pulse applied by the PFM tip to the pristine (as-grown) domain. To avoid charge injection, which could lead to unwanted backswitching effects,[21] the tip was lifted up right before the end of each pulse. Most of the earlier PFM studies of polarization reversal were carried out by monitoring the field-induced changes in the domain structure imaged on the polar surface.[22,23] Those experiments provided valuable information about the sideways domain growth (in the direction perpendicular to the polar axis), whereas the forward growth (along the polar direction) remained unattainable. However, recent theoretical and experimental reports have demonstrated a possibility of polarization control and domain visualization on the non-polar surface (parallel to the polar axis) due to the lateral components of the electric field generated by a PFM probe.[21,24–26] This approach has the specific advantage of inducing and detecting the domain growth both in the sideways and forward directions by employing the lateral PFM mode.[27,28] Most importantly, visualization of the growing domains on the non-polar surface allows comparative analysis of the difference in the electric field driven kinetics and stability of the electrically neutral and nominally charged domain walls.

Experimental results reveal quite unconventional domain growth behavior on the non-polar surface of PGO (**Figure 3**). Previous studies on the non-polar surfaces of $LiNbO_3$ and diisopropylammonium bromide (DIPA-B) crystals showed that voltage pulse application typically leads to the formation of wedge-shaped domains extending primarily in the polar direction.[26] The length–width aspect ratio of these domains was usually close to 10 resulting from a significant difference between the forward and sideways domain growth velocities (here the length refers to the domain size in the polar direction and the width refers to the size along the direction normal to the polar axis). In contrast, in PGO, the growing domain expands preferentially in the direction normal to the polar axis as is illustrated by the voltage-dependent evolution of the growing oblate domain in Figure 3a. This trend is even more evident in the time-dependent PFM patterns shown in Figure 3b, where the length–width ratio of the largest grown domain is as low as 0.3. Results of the PFM data analysis are summarized in Figures 3c,d. A similar domain switching behavior has been observed for the opposite voltage polarity (see Section S3 and Figure S3, Supporting Information).

To understand the reason for this unconventional domain switching behavior obtained on the non-polar surface, we used phase-field modeling (see Section S4, Supporting Information, for details). It has been previously proposed that screening of the bound polarization charges at the H–H and T–T domain walls plays an important role in determining the shape of the growing domains.[21,26] To clarify the role of bound polarization charges and screening effects in the observed domain switching behavior in PGO, we simulated two extreme cases.

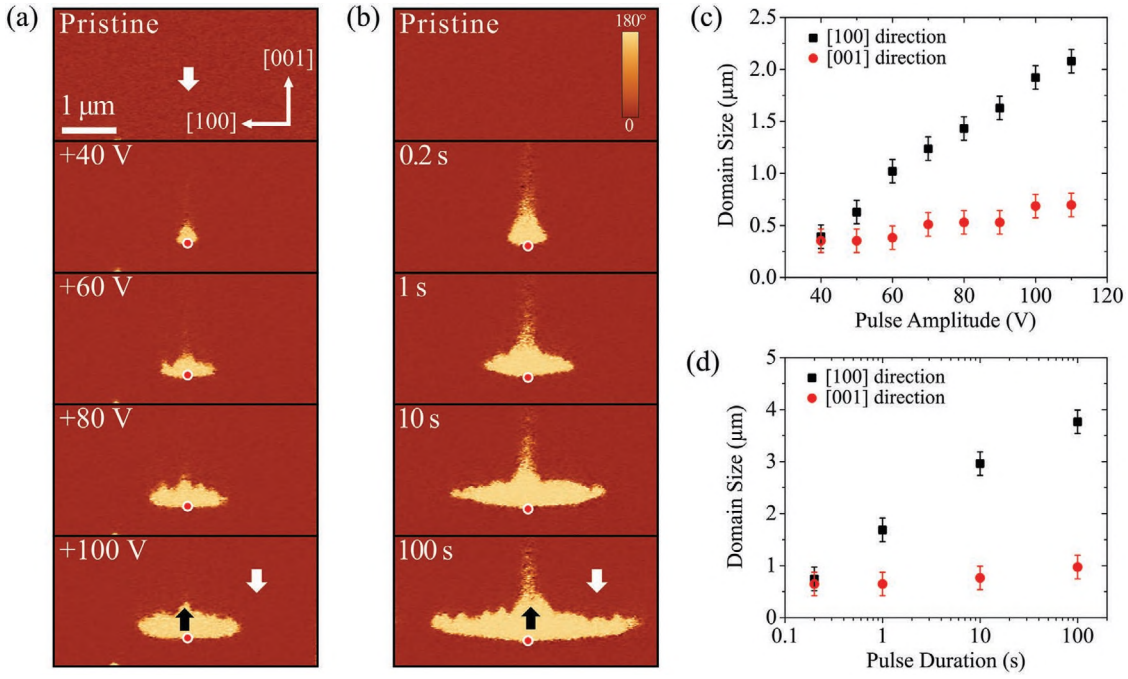


**Figure 3.** PFM phase images of the domain growth dynamics a) as a function of the pulse amplitude, and b) as a function of the pulse duration. The tip position during pulse application is marked by the red dots. c) Pulse amplitude and d) pulse duration dependences of the domain sizes along different crystallographic directions determined from the PFM data. Pulse duration in (a) and (c) is fixed at 0.2 s. Pulse amplitude in (b) and (d) is fixed at +60 V. Pulses were applied to the pristine (as-grown) domain.

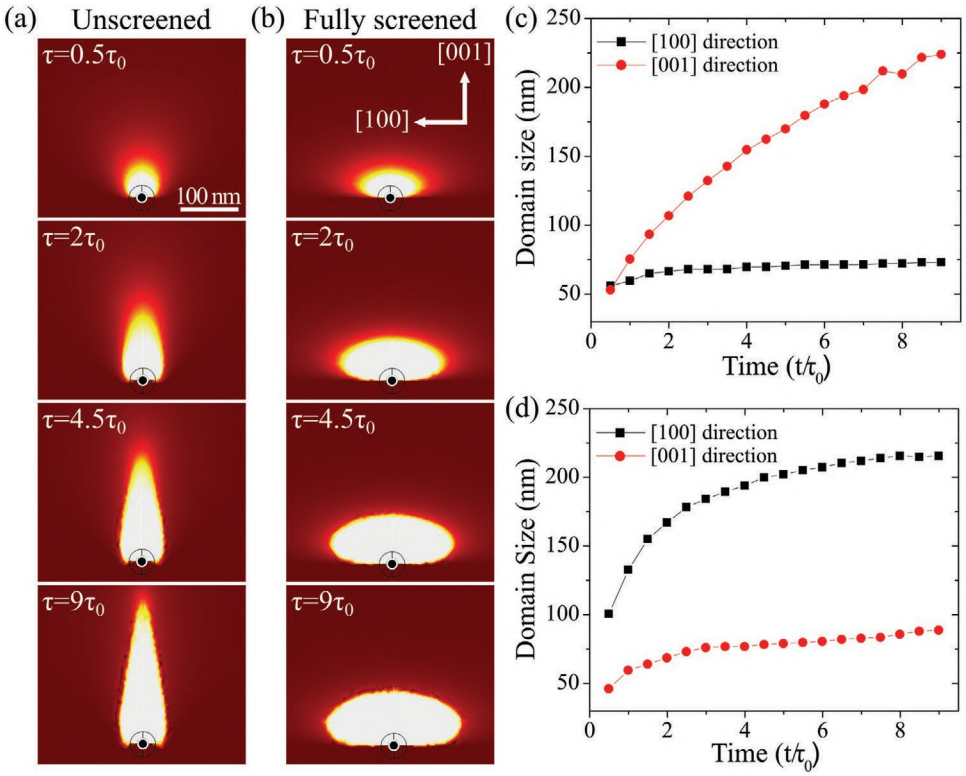


**Figure 4.** Phase-field modeling of the domain growth dynamics on the non-polar surface of PGO. Domain configurations at different time intervals for the a) unscreened and b) completely screened H–H domain wall. Domain size as a function of time for the c) unscreened and d) completely screened H–H domain wall. The tip bias for this modeling is fixed at 30 V.

In the first scenario, no screening of the polarization charges at the H–H and T–T domain walls took place (this corresponds to $\rho = 0$, where $\rho$ is the screening charge density). The simulated snapshots of the growing domain during the tip-induced switching are shown in **Figure 4**a. In the second scenario, we considered a system where the polarization charges at the H–H or T–T domain walls were fully screened (so that $\rho = \partial P_z/\partial z$), which yielded the simulation results shown in Figure 4b. A significant difference between the shapes of the growing domains can be clearly seen. In the first case, with no screening, the domain grows much faster along the polar axis (Figure 4c) thereby acquiring a wedge shape, which is similar to the growth behavior reported in $LiNbO_3$[29] and DIPA-B.[26] In the second case, corresponding to the complete screening of the H–H and T–T domain walls, the domain expands in the direction normal to the polar axis (Figure 4d), which is consistent with the experimental results observed here. Figure S4, Supporting Information, illustrates a gradual transformation of the simulated domain shapes due to the varying degree of the polarization charges screening at the H–H domain wall in PGO. For reference, similar modeling was carried out for tip-generated domains on the non-polar surface of $LiNbO_3$ (Figure S5, Supporting Information). On the one hand, it can be seen that in the absence of screening of the charged H–H domain walls, the growing domains evolve into a wedge extended in the polar direction (Figure S5a, Supporting Information) in agreement with the earlier experimental reports.[29] On the other hand, if the polarization bound charges are completely screened, then the oblate domain will form extending preferentially in the direction normal to the polar axis, which is similar to the behavior observed in PGO (Figure S5b, Supporting Information).

## 3. Conclusion

Thus, based on the phase-field modeling results, we have to assume that the H–H and T–T domain walls are either fully screened or, alternatively, do not exhibit bound charges. Note that this type of domain walls in PGO has not been investigated at the atomic scale so that their inner structure remains unknown. While complete screening of the domain walls could be justified in some way for the as-grown PGO crystals, for example, through long-term accumulation of mobile defects on the charged walls, it is not reasonable to expect full screening for the micrometer long charged domain walls generated by the tip-induced field (PGO is a semiconductor with a bandgap of 3.0 eV). Furthermore, in contrast to other ferroelectrics with charged domain walls, the Kelvin probe force microscopy and electrostatic force microscopy (EFM) studies performed on the same samples do not detect any trace of the bound charges at the H–H and T–T domain walls (Figure S6, Supporting Information). Neither do these walls exhibit any conducting behavior even in the crystals with sub-micrometer thickness as is established by conducting atomic force microscopy measurements (Figure S6, Supporting Information). We thus conclude, that

the H–H and T–T domain walls in PGO are not inherently charged. This conclusion brings about an important question related to crystal and electronic structure of the domain walls in PGO, which can possibly be addressed by high spatial resolution electron energy loss spectroscopy measurements and first-principle modeling. At this point, it is reasonable to assume that the structure of the domain walls in PGO is fundamentally different from the conventional Ising-type structure, which might be related to the enantiomorphic nature of $Pb_5Ge_3O_{11}$.

Another possibility is that the domain structure in PGO consists of microscopically long, wiggled, and twisted filament-like antiparallel domains extended along the [001] direction. When these domains are about to meet head-to-head or tail-to-tail, polarization deviates from the [001] crystallographic direction to avoid formation of the charged H–H and T–T domain walls and to maintain the continuity of the polarization. As a result, the domains bend and split but never terminate within the bulk of the sample although at the expense of the increased anisotropy energy. The quenched polar defects would further promote formation of the intertwined filament domains. Intersection of this challah-like domain structure with the non-polar surface would produce a domain pattern similar to the one shown by the PFM image in Figure 1b.

In general, our study shows that the physics of nominally charged domain walls goes way beyond a specific conductance behavior requiring a deeper insight into the dynamics-related phenomena associated with domain formation. The reported finding is of interest for other wide-band-gap semiconducting ferroelectrics, where mobile charge carriers are rare and cannot be readily excited over the bandgap to compensate bound polarization charges suggesting non-trivial static and dynamic properties of the nominally charged domain boundaries.

## Supporting Information

Supporting Information is available from the Wiley Online Library or from the author.

## Acknowledgements

Research at the University of Nebraska (SPM measurements) was supported by the National Science Foundation (NSF) grant DMR-1709237 and through the Nebraska Materials Research Science and Engineering Center (MRSEC, grant DMR-1420645). The work at Penn State University (phase-field modeling) was supported by the NSF MRSEC (grant DMR-1420620) and by the NSF grant DMR-1744213. The work at Argonne National Laboratory (V.M.V.) was supported by the U.S. Department of Energy, Office of Science, Basic Energy Sciences, Materials Sciences and Engineering Division. I.L. acknowledges the support of the European Horizon 2020 projects: MSCA-RISE Materials for Neuromorphic Circuits and MSCA-ITN Memristive and Multiferroic Materials for Emergent Logic Units in Nanoelectronics. Research at NTNU (SPM measurements) was supported through the Onsager fellowship program. Research at QUB was supported by the EPSRC (grant no. EP/P02453X/1) and the US-Ireland R&D Partnership Programme (grant no. USI 120).

## Conflict of Interest

The authors declare no conflict of interest.

## Keywords

ferroelectric domain walls, lead germanate, phase transition, piezoresponsive materials, polarization reversal

[1] A. Gruverman, M. Alexe, D. Meier, *Nat. Commun.* **2019**, *10*, 1661.
[2] J. Seidel, L. W. Martin, Q. He, Q. Zhan, Y.-H. Chu, A. Rother, M. E. Hawkridge, P. Maksymovych, P. Yu, M. Gajek, N. Balke, S. V. Kalinin, S. Gemming, F. Wang, G. Catalan, J. F. Scott, N. A. Spaldin, J. Orenstein, R. Ramesh, *Nat. Mater.* **2009**, *8*, 229.
[3] D. Meier, J. Seidel, A. Cano, K. Delaney, Y. Kumagai, M. Mostovoy, N. A. Spaldin, R. Ramesh, M. Fiebig, *Nat. Mater.* **2012**, *11*, 284.
[4] M. Schröder, A. Haußmann, A. Thiessen, E. Soergel, T. Woike, L. M. Eng, *Adv. Funct. Mater.* **2012**, *22*, 3936.
[5] H. Lu, Y. Tan, J. P. V. McConville, Z. Ahmadi, B. Wang, M. Conroy, K. Moore, U. Bangert, J. E. Shield, L.-Q. Chen, J. M. Gregg, A. Gruverman, *Adv. Mater.* **2019**, *31*, 1902890.
[6] E. I. Speranskaya, *Zh. Neorg. Khim.* **1960**, *5*, 421.
[7] H. Iwasaki, K. Sugii, T. Yamada, N. Niizeki, *Appl. Phys. Lett.* **1971**, *18*, 444.
[8] A. Gruverman, N. Ponomarev, K. Takahashi, *Jpn. J. Appl. Phys.* **1994**, *33*, 5536.
[9] V. Y. Shur, A. Gruverman, E. L. Rumyantsev, *Ferroelectrics* **1990**, *111*, 123.
[10] S. Nanamatsu, H. Sugiyama, K. Dol, Y. Kondo, *J. Phys. Soc. Jpn.* **1971**, *31*, 616.
[11] H. Iwasaki, K. Sugii, *Appl. Phys. Lett.* **1971**, *19*, 92.
[12] J. P. Dougherty, E. Sawaguchi, L. E. Cross, *Appl. Phys. Lett.* **1972**, *20*, 364.
[13] V. Y. Shur, A. Gruverman, V. V. Letuchev, E. L. Rumyantsev, A. L. Subbotin, *Ferroelectrics* **1989**, *98*, 29.
[14] C. Dasgupta, R. Pandit, *Phys. Rev. B* **1986**, *33*, 4752.
[15] R. Schilling, *J. Stat. Phys.* **1988**, *53*, 1227.
[16] T. Castán, P. A. Lindgård, *Phys. Rev. B* **1989**, *40*, 5069.
[17] I. M. Lifshitz, *J. Exp. Theor. Phys.* **1962**, *15*, 939.
[18] S. M. Allen, J. W. Cahn, *Acta Metall.* **1979**, *27*, 1085.
[19] Q. N. Meier, M. Lilienblum, S. M. Griffin, K. Conder, E. Pomjakushina, Z. Yan, E. Bourret, D. Meier, F. Lichtenberg, E. K. H. Salje, N. A. Spaldin, M. Fiebig, A. Cano, *Phys. Rev. X* **2017**, *7*, 041014.
[20] V. Y. Shur, E. L. Rumyantsev, A. L. Subbotin, *Ferroelectrics* **1993**, *140*, 305.
[21] A. V. Ievlev, D. O. Alikin, A. N. Morozovska, O. V. Varenyk, E. A. Eliseev, A. L. Kholkin, V. Y. Shur, S. V. Kalinin, *ACS Nano* **2015**, *9*, 769.
[22] B. J. Rodriguez, R. J. Nemanich, A. Kingon, A. Gruverman, S. V. Kalinin, K. Terabe, X. Y. Liu, K. Kitamura, *Appl. Phys. Lett.* **2005**, *86*, 012906.
[23] A. Agronin, M. Molotskii, Y. Rosenwaks, G. Rosenman, B. J. Rodriguez, A. I. Kingon, A. Gruverman, *J. Appl. Phys.* **2006**, *99*, 104102.
[24] N. A. Pertsev, A. L. Kholkin, *Phys. Rev. B* **2013**, *88*, 174109.
[25] F. Kagawa, S. Horiuchi, N. Minami, S. Ishibashi, K. Kobayashi, R. Kumai, Y. Murakami, Y. Tokura, *Nano Lett.* **2014**, *14*, 239.
[26] H. Lu, T. Li, S. Poddar, O. Goit, A. Lipatov, A. Sinitskii, S. Ducharme, A. Gruverman, *Adv. Mater.* **2015**, *27*, 7832.
[27] A. Gruverman, S. V. Kalinin, *J. Mater. Sci.* **2006**, *41*, 107.
[28] T. Jungk, A. Hoffmann, E. Soergel, *New J. Phys.* **2009**, *11*, 033029.
[29] D. O. Alikin, A. V. Ievlev, A. P. Turygin, A. I. Lobov, S. V. Kalinin, V. Y. Shur, *Appl. Phys. Lett.* **2015**, *106*, 182902.